Journal of Cleaner Production 279 (2021) 123541

Contents lists available at ScienceDirect

Journal of Cleaner Production

journal homepage: www.elsevier.com/locate/jclepro

Pyrolysis of excavated waste from landfill mining: Characterisation of the process products

Katarzyna Jagodzińska *, Ilman Nuran Zaini , Rikard Svanberg , Weihong Yang , Pär Göran Jönsson

KTH Royal Institute of Technology, Department of Material Sciences and Engineering, Brinellvägen 23, Stockholm, Sweden

ARTICLE INFO

Article history:
Received 20 April 2020
Received in revised form
29 July 2020
Accepted 31 July 2020
Available online 12 August 2020

Handling Editor: Bin Chen

Keywords:
Enhanced landfill mining
Waste management
Waste to energy
Circular economy
GC/MS
RDF

ABSTRACT

The current transition to a circular economy model laid the foundations for the development of the Enhanced Landfill Mining concept. Hitherto, a few studies have been performed on the thermochemical valorisation of excavated waste, of which a majority concern incineration or gasification. Nonetheless, no previous studies on excavated waste pyrolysis, including the characterisation of the process products, have been identified. Ergo, this study aims at filling this knowledge gap. The pyrolysis of refuse-derived fuel formed from excavated waste was performed in a lab-scale reactor in the temperature range of 400 −700 °C. The non-condensable products (non-condensables) were analysed using Micro GC, whereas the condensable products (condensables) were characterised using GC/MS. Additionally, the distribution of C, H, N, S, O, and Cl among the process products was analysed. The high content of C_2−C_3 hydrocarbons was detected in non-condensables, whereas the abundance of polycyclic aromatic hydrocarbons (PAHs) was detected among condensable products. However, due to feedstock complex thermal decomposition pattern, no overall tendency, covering the process product properties in relation to the process temperature, can be determined. These fluctuations of composition, therefore, have to be taken into account in the planning of the future utilisation of the excavated waste pyrolysis products. Moreover, two possible risks, connected with the further process products utilisation, were identified − namely, chlorine forming primarily organic compounds and sulphur forming mostly gaseous compounds (H_2S).

1. Introduction

Undeniably, the world is facing an unprecedented challenge of stimulating economic growth and simultaneously maintaining its sustainability. This directly leads to a transition to resource and energy efficiency technologies based on a circular economy approach. As stated by (Jones et al., 2013), closing of material loops, in a circular economy way, can be done by direct recycling of pre-consumer residues (e.g., residues from steel production process), urban mining of post-consumer residues (e.g., electronic waste as a source of rare metals), and mining of existing (and future) landfills.

Mining of existing and future landfills can result in a substantial stream of secondary materials and energy, reducing, at the same time, the area they cover. Consequently, landfill mining corresponds with the European Union's Roadmap to a Resource Efficient Europe (European Commission, 2011), which includes no net land take by 2050, thereby dragging land into the group of resources that have to be sustainably managed. Nevertheless, it is not just the EU that faces the need to secure more land for landfills - the challenge exists worldwide - among others, in China (Zhou et al., 2014), South Korea (Yi, 2019), India (Singh and Chandel, 2019) or Indonesia (Lokahita et al., 2019). Thus, landfill mining is seen as a way to mitigate the problem. It aroused much interest as an attractive source of rare metals (Kamura et al., 2019), but also as a tool for alleviating the negative environmental impact of landfills as they are the sources of air, soil and groundwater pollution, for instance, with microplastics (He et al., 2019).

The landfill mining concept was introduced in the early 50s in Israel as a source of soil fertilisers. The idea, however, attracted the attention of the international community only in the early 90s. The first project related to the concept started in 1993 in Germany, and a significant number of such projects were launched in the United

Abbreviations: ELFM, Enhanced Landfill Mining; DTG, derivative thermogravimetric; GC, gas chromatograph; MS, mass spectrometer; RDF, refuse-derived fuel; PAHs, polycyclic aromatic hydrocarbons; TG, thermogravimetric.

* Corresponding author.
E-mail address: kjag@kth.se (K. Jagodzińska).

https://doi.org/10.1016/j.jclepro.2020.123541

States and Canada as well (Hogland et al., 2004). Besides, between 1995 and 2010, five Swedish landfills were, partially or entirely, excavated (Johansson et al., 2012). The motivations of the aforementioned projects were mostly land reclamation and end of landfills' operational life. The dominating way of energy recovery from buried materials was their incineration.

Indeed, excavated waste incineration is often considered as the most suitable way of their valorisation (Quaghebeur et al., 2013; Zhou et al., 2014). However, not only is it not covered by a greater objective of the circular economy, but it is also connected with numerous technical complications. According to (Forster, 1995), high soil-like fines content in excavated waste results in an increase of the abrasion intensity for feeding equipment (e.g., feed chute hoppers) and flue gas ducts in incineration plants. It also contributes to overstressing the loading equipment (cranes), because of the higher density of such fuels (Rotheut and Quicker, 2017). Encountered problems with maintaining stable incineration parameters because of abnormalities with fire propagation and uneven distribution of the fuel over a grate. That caused fluctuations in the steam production and, eventually, the breakdown of the combustion process. Furthermore, in both mentioned studies, significantly higher emissions of HCl were noted (Forster, 1995; Rotheut and Quicker, 2017).

Since the landfill mining concept had been limited mostly to land reclamation and incineration of excavated waste, in 2008, a new concept was developed – the so-called Enhanced Landfill Mining (ELFM), addressing the need for actions against progressive planet degradation and climate change. Following (Jones et al., 2013), ELFM comprises valorisation of excavated waste as both materials and energy, complying with rigorous ecological regulations and social criteria. ELFM, however, is also associated with noise and dust emissions, visual disturbances for animals, and temporary losses of habitats. Notwithstanding that, compared to the 'do-nothing' scenario, ELFM offers a reduction of CO_2 emissions of 1 million t over 20 years, due to the limitation of materials needed to be produced (Jones et al., 2013).

Hitherto, research on both landfill mining and enhanced landfill mining was primarily focused on the characteristic of excavated material and the technology used for excavation and sorting (Krook et al., 2012). The characteristic of excavated waste varies, depending on, among others, type of buried waste (e.g., municipal solid waste, industrial waste), climate, location, and type of landfill, age of excavated waste, pH of leachate (Hogland et al., 2004; Kaartinen et al., 2013; Ximenes et al., 2018). However, some common denominators can be found, namely, high content of soil-like fines, moisture and contaminants (e.g., heavy metals), and relatively low calorific value. Since the feedstock can be considered as a demanding and site-specific, suitable technology for its recovery has to be individually tailored. Moreover, frequently, a dedicated pre-treatment (e.g., sorting, screening, shredding, pelletising, drying) has to be implemented before the valorisation process (Bosmans et al., 2013; Zhou et al., 2014).

Only a few studies discussed the technical possibilities of excavated waste valorisation via thermochemical route. Plasma technologies were indicated as promising ways of excavated waste valorisation, resulting in a high-quality syngas production alongside a vitrified material, which can be used as a construction material or a high-end product (e.g., bricks) (Danthurebandara et al., 2015). Indeed (Agon et al., 2016), performed plasma gasification of refuse-derived fuel (RDF) from excavated waste and obtained syngas with a promising characteristic and a low tar content, albeit failed with providing a valuable vitrified product.

(Canopoli et al., 2018), on the other hand, indicated that pyrolysis is as a viable and cost-effective way of excavated waste valorisation, nonetheless emphasised the need for more research on the process. A thorough search of the relevant literature yielded only two related articles (Bosmans et al., 2014). Studied kinetics of excavated waste pyrolysis, and proved that their thermal decomposition does not reflect the thermal decomposition pattern of fresh waste. Independently (Breyer et al., 2017), performed co-pyrolysis of excavated plastics with used lubrication oils to produce an alternative fuel for cement kilns. The goal was achieved with a maximum content of excavated plastic of 60 wt%, and the authors claimed that the process is economically viable from an energetic point of view.

The aforementioned knowledge gap motivated this study. To the best of our knowledge, this is the first study on excavated waste pyrolysis with a complex characterisation of the process products. The process was performed at six temperatures in the range of 400–700 °C. Consequently, the temperature impact on the quality of the process products was determined. The feedstock used within the study was RDF made of waste excavated from an existing Belgian landfill site.

2. Material and methods

2.1. Feedstock properties

The refuse-derived fuel (RDF) used within the study was formed from waste excavated at the Mont-Saint-Guibert landfill in Belgium (Garcia Lopez et al., 2019). Approximately 5.7 mln m^3 of construction and demolition waste, municipal solid waste, and non-hazardous industrial waste were disposed at the landfill from 1958 to 1985. That old part of the landfill was subjected to excavation, which resulted in the collection of approximately 130 m^3 of the buried material. Thereafter, the material was ballistically sorted using a commercial scale separator (STT6000, Stadler Anlagenbau GmbH). As a result, three fractions were obtained, namely light, heavy, and fine fractions.

The light fraction (particle size of 90–200 mm) showed the highest potential for an energy use, due to its high heating value and relatively low impurities content. Hence, it was selected for the pyrolysis tests within the study.

Table 1 shows the feedstock's composition (Garcia Lopez et al., 2019). The distinguished fractions do not have the specified composition – the wood fraction consists of all types of wood, as well as textiles of all kinds of textiles, both synthetic and natural. The paper fraction mainly consist of composite carton and cardboard, but also other types of paper can be found in it. The so-called 2D plastic fraction is primarily made of thin foil and plastic bags, whereas the 3D plastic consists of thick PS, PP, PE, PVC debris. The remaining fraction (further referred to as the *rest* fraction) is a mixture of foam, rubber, EPS, hazardous waste like sanitary material, and other, unidentified components. The inert fraction consists of ceramic and mineral fractions. So does the fines fraction, which has an ash content of approx. 88 wt% (Garcia Lopez et al., 2019).

Table 1
Composition of the feedstock in a dry state (Garcia Lopez et al., 2019).

Fraction	Content, wt%
Wood	0.7
Paper	3.5
Textile	8.4
2D plastics	37.5
3D plastics	4.8
Ferrous metals	1.7
Non-ferrous metals	0.2
Inert	1.5
Rest	10.5
Fines (particles < 20 mm)	31.2

Prior to the tests, it was necessary to reduce the fractions' particle sizes to improve their homogeneity and to enable the performance of lab-scale tests with certain repeatability. Several mills were used (hammer, disc, and cutting mill) and the final particle size of the used feedstock was smaller than 3 mm.

An external lab (Eurofins Biofuel & Energy Testing Sweden AB, Lidköping, Sweden) determined the feedstock elemental composition – C, H, N following the EN 15407:2011 standard, S and Cl following the EN 15408:2011 standard, the moisture following the EN 15414–3:2011 standard, and the ash content following the EN 15403:2011 standard, and calculated the oxygen content as difference. The results of the analysis are shown in Table 2. In comparison to RDF formed from municipal solid waste or from industrial waste, the analysed RDF is characterized by high ash, sulphur and chlorine contents (Jagodzińska et al., 2019b; Sieradzka et al., 2020), which may be problematic during its energetic utilisation (Nobre et al., 2019).

2.2. Thermogravimetric analysis

The experimental campaign started with a thermogravimetric analysis (STA 449 F1 Jupiter, NETZSCH) to initially choose the process temperature. The procedure was as follows: heating at 5 °C/min to 300 °C, holding at 300 °C for 5 min, then heating at 10 °C/min to 850 °C, and holding for 10 min. The reacting atmosphere was inert due to the nitrogen flow rate of 50 ml/min. The sample mass varied between 20 mg and 70 mg - the buoyancy effect was observed for the lightest sample (20 mg), and for that reason, the sample mass was increased. Tests were repeated three times to ensure the repeatability of the measurements. The standard deviations for thermogravimetric (TG) and derivative thermogravimetric (DTG) profiles were, on average, 2 wt% and 0.2 wt%/min, respectively.

The average TG and DTG profiles are shown in Fig. 1. One main asymmetric (leading) peak, corresponding to the maximal mass loss, can be observed in the temperature range of 400–500 °C. Therefore, this temperature range was chosen within the study with an additional intermediate step at 450 °C. This temperature range complied with the study of (Bosmans et al., 2014), where a mixture of excavated municipal solid waste and industrial waste was pyrolysed.

2.3. Trial tests and process temperature

After the thermogravimetric analysis (TGA), a set of trial tests in the fixed-bed reactor was performed (Fig. 2). The reactor is described further in the *2.4 Pyrolysis tests* section. The trial tests revealed that the sample mass loss still occurs at higher temperatures of approx. 100 °C than those indicated by the thermogravimetric (TG) measurements. The discrepancy can be attributed to the different heat transfer conditions, especially the heating rate and sample mass, which are higher in the fixed bed reactor

Table 2
Proximate and elemental compositions of the feedstock (dry basis).

Compound/element	Content, wt%
ash	46.48 ± 4.65
moisture	1.5 ± 0.15
C	40.5 ± 2.025
H	6.1 ± 0.61
N	1.1 ± 0.11
S	0.234 ± 0.023
Cl	1.203 ± 0.301
O (calculated)	4.3

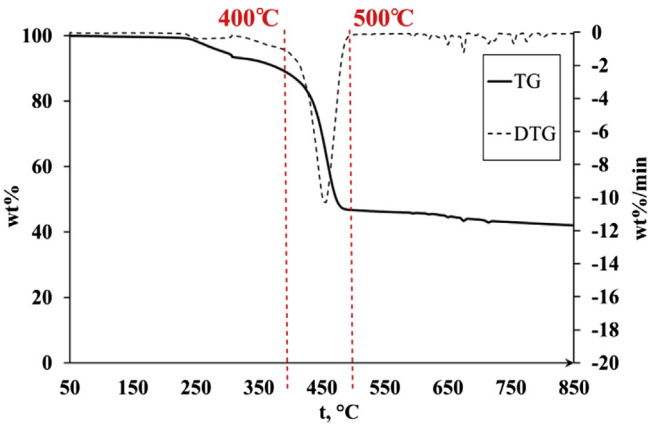

Fig. 1. TG and DTG profiles for RDF from excavated waste under a nitrogen atmosphere.

compared to that of the TG experiment. The higher mass combined with higher heating rate results in higher heat transfer resistances (Bosmans et al., 2014). Additionally, the feedstock itself is characterised by a relatively high heating resistance due to the high soil-like fraction content (*inert* and *fines* fractions in Table 1). Consequently, a considerable thermal lag occurs, and the heat necessary for sample devolatilisation is reached at a higher temperature compared to the TGA, which results in the shift of the pyrolysis profile (Manyà et al., 2015). A similar phenomenon was observed by (Bosmans et al., 2014), where the merging of TG peaks occurred when the heating rate was increased.

Given the above, the process temperature range mentioned in paragraph *2.2 Thermogravimetric analysis* (400 °C, 450 °C and 500 °C) was extended to include 550 °C, 600 °C and 700 °C.

2.4. Pyrolysis tests

The tests were performed in a fixed bed reactor shown in Fig. 2. The test rig is made up of an electrically heated reactor (stainless-steel; inner diameter of 24 mm) equipped with a condensing section (a cooling jacket, four impingers immersed in a cooling bath, and an impinger with deionised water to collect HCl), and an aerosol trap. The reactor is heated by the ceramic insulated band heaters. The temperature in the reactor is regulated by a proportional–integral–derivative (PID) controller, which is connected with the thermocouple placed between the ceramic insulated band heater and the reactor tube. The reaction temperature is controlled by the thermocouple immersed in the sample ceramic basket.

The reactor has a cooling zone at its upper extension. The cooling agent at −15 °C (isopropanol/deionised water mixture with the volume ratio of 75/25) circulates between the cooling bath, the cooling jacket, and the cooling zone tubing. The reactor is flushed with nitrogen to ensure an inert atmosphere of the reaction and to simultaneously act as a carrier medium for the produced vapours. The mixture of nitrogen and produced pyrogas flows through the condensing section, where condensable compounds are collected. The non-condensable compounds (non-condensables) flows further to the Micro GC (490 Micro GC System QUAD, Agilent), where their composition is monitored on-line. Afterwards, their flow is measured by a drum-type gas meter (TG1 type, Ritter, Germany), and, subsequently, they are collected in a Tedlar™ gas sample bag to enable a determination of their total composition.

The test procedure was as follows: first, 2 g of the dried sample (dried at 80 °C overnight) was placed in the cooling zone and then the reactor was heated to the chosen temperature. When the

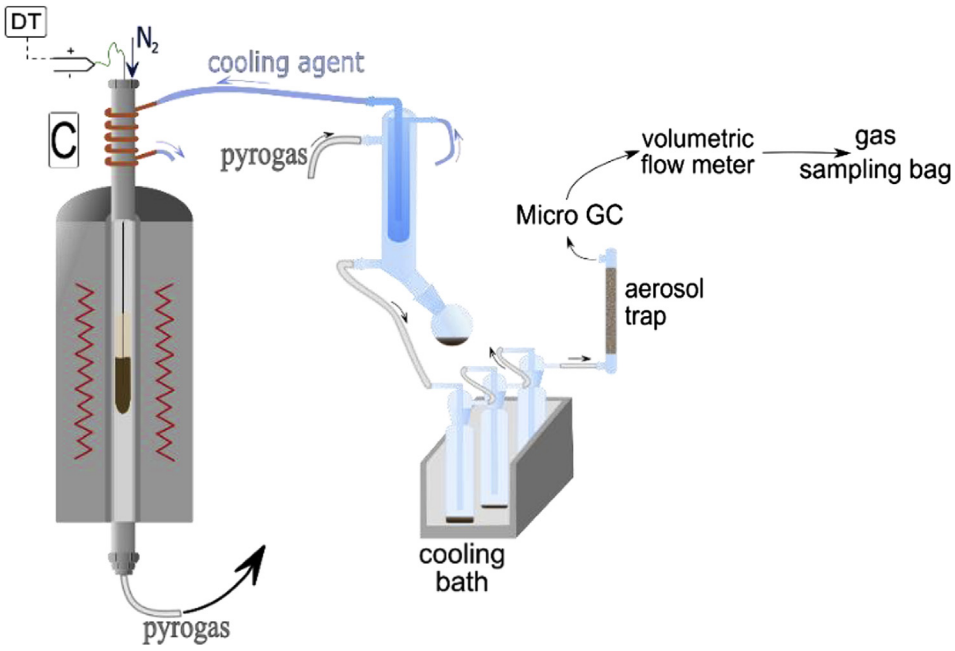

Fig. 2. A general scheme of the test rig (C – cooling zone; DT – digital thermometer).

temperature reached the desired level, the sample was promptly introduced to the hot reactor. Since the beginning, the reactor was flushed with nitrogen (100 ml/min). The sample was kept in the hot reactor for 30 min, after which it was pulled up to the cooling zone, and the reactor was flushed until the Micro GC did not detect any pyrolysis gas (usually 15–30 min). The cooling jacket, impingers, and aerosol trap were sealed and weighted immediately after the experiment to prevent the evaporation of highly volatile products. The sample basket, the condensing section, and the aerosol trap were weighed before and after the experiment to determine product yields. Eventually, the mass balance closure was done by calculating the non-condensables mass from their known composition and flow.

The tests were repeated at least 3 times to ensure a repeatability of the results. Moreover, a random order of experiments was introduced to ensure avoidance of consecutive run errors.

2.5. Pyrolysis products characterisation

The collected condensables were in the form of a very thin wax-like layer on the glassware walls, but they dissolved in DCM/methanol solution (volume ratio of 50/50), which enabled their collection. The water content of the condensables, analysed by Karl Fischer titration (T5 titrator, Meter Toledo), did not exceed 2%.

The composition of condensables was analysed using GC/MS (Agilent 7890A/Agilent 5975C) with a DB-1701 column (30 m × 0.25 mm × 0.25 μm, Agilent). The MS scanning range was m/z 45–550, with a frequency of 1.6 scans/sec. The MS source and quadrupole temperatures were 230 °C and 150 °C, respectively. Samples were introduced to the GC injector at 280 °C (splitless) with helium as a carrier gas (1 ml/min). The temperature profile was as follows: holding at 35 °C for 5 min, heating with 5 °C/min to 250 °C, and holding for 10 min. The identification of the compounds was done automatically with a minimum match factor with the NIST-11 library of 75%. After that, the results of repetitions were compared, and the identification of the compounds was verified manually. The results of the GC/MS analysis are shown in the form of weight-normalised area% to enable comparison of the samples and identification of trends. The weigh-normalisation was done by dividing area by the weight of condensables from each experiment.

The collected non-condensables were analysed using the Micro GC (490 Micro GC System QUAD, Agilent), equipped with Molsieve 5 Å, PoraPLOT U, Al_2O_3/KCl, and CP-Sil 5CB columns. The Micro GC was calibrated for N_2, O_2, H_2, CH_4, CO, CO_2, H_2S, and C_2–C_4 hydrocarbons.

The ash content in the char was analysed following the EN-ISO 18122:2015 standard. Moreover, an external lab (Zakłady Pomiarowo-Badawcze Energetyki „ENERGOPOMIAR" Sp. z o. o., Gliwice, Poland) analysed the char elemental composition - C, H, N and S contents using infrared and thermal conductivity detector following the EN 15407:2011 standard, and Cl content using an ion chromatography following the EN 15408:2011 standard. Knowing the ash, C, H, N, S, and Cl contents in the char, the oxygen content in the char was calculated by difference. The external lab also analysed Cl content in the deionised water from the last impinger in the condensing section, using ion chromatography following the EN ISO 10304–1:2009 +AC:2012 standard. This chlorine content is considered to be the total chlorine content in the non-condensables.

The known composition of non-condensables and char enabled a calculation of the elements balances (C, H, N, S, Cl, and O). Unfortunately, the form of the condensables demanded their collection using the solvent; therefore, the analysis of their elemental composition was impossible. In consequence, the C, H, N, S, Cl, and O contents in condensables were calculated as the difference between the initial element content and its content in char and non-condensables.

2.6. Limitations of the study

As with the majority of studies, this study is subject to limitations. Two major limitations could be addressed in future research, whereas the third one identifies the need for further development in the area of study.

The first limitation concerns the GC/MS analysis that resulted in a relatively high content of unknown compounds (up to 11% of the

weight-normalised area in Fig. 5). In further studies, either more efficient separation technique (e.g. 2D GC) or initial fractionation of the condensables shall be performed to improve identification of the compounds.

The second limitation is related to the condensables collection with DCM/MeOH solution. Using the solvent excluded the possibility of C, H, N, S, Cl and O contents determination in the condensables. Therefore, the closure of the elements mass balance was based on the calculation of their content in the condensables. In future research, the condensation system shall be modified to intensify condensation at its beginning, thereby increasing the thickness of condensables' layer in the initial part of the system. This would allow the partial collection of condensables without using any solvent.

The last limitation is related to the lack of previous studies on excavated waste pyrolysis. For this reason, there is a lack of data to refer to and compare with the obtained results.

3. Results

3.1. Product yields

The mass balances for pyrolysis at different temperatures are shown in Fig. 3 and the exact yield values are shown in Table A1 in the Supplementary material. With a temperature increase, the char yield decreases nearly linearly in favour of the pyrovapours (condensables and non-condensables) yield. The char yield has its minimum at 600 °C, and a further increase of the process temperature does not result in char mass loss greater than the margin of error. These results coincide with available data (Hwang et al., 2014; Montané et al., 2013).

On the contrary, the change of condensables and non-condensables yields with a temperature variation is non-linear. In general, it can be seen that condensables are predominantly formed and that their yield increases with a temperature increase, except for two temperatures - 550 °C and 700 °C where non-condensable yield has its local maxima. The local maximum at 550 °C is related to the character of the process and occurring reactions, whereas the local maximum at 700 °C is related to the thermal cracking of condensables into non-condensables. The obtained data is inconsistent with the available literature data (Buah et al., 2007; Chen et al., 2015), where condensables and non-condensables yields show overall increasing tendencies without fluctuations along with the temperature profile. The sample mass loss at 550 °C can be principally linked to the decomposition of mixed plastics in the sample. According to (Williams and Williams, 1999a), interactions between different types of plastics (PE, PP, PS, PVC) results in the production of higher non-condensables yield comparing to the individual plastics pyrolysis. Therefore, the above mentioned shift at 550 °C can be attributed to the extensive decomposition of different plastic types. Moreover, the high degradation degree of the plastics found in excavated waste (Canopoli et al., 2020) can change their thermal behaviour and lead to the formation of more non-condensable compounds.

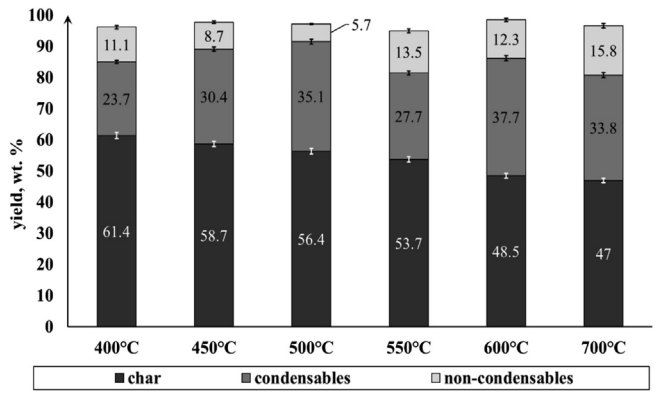

Fig. 3. Pyrolysis product yields at different temperatures.

3.2. Non-condensables composition

Fig. 4 shows the non-condensables composition at different pyrolysis temperatures. The measured hydrocarbons were divided into three groups, namely C_2 gases (C_2H_6, C_2H_4, C_2H_2), C_3 gases (C_3H_8, C_3H_6), and C_4 gases (C_4H_{10}, C_4H_8). The exact values are shown in Table A2 in the Supplementary material.

The results do not show one overall tendency in accordance with the temperature changes. This is connected to the feedstock's complex composition and, consequently, complex thermal decomposition pattern. Results at temperatures below 400 °C are generally linked to lignocellulosic fraction decomposition, whereas those above 400 °C occur due to plastics decomposition (Bosmans et al., 2014). In the analysed feedstock, the plastics fraction dominate, followed by the so-called *rest* fraction (foam, rubber, etc.) and textiles, whereas content of the paper and wood fractions is low. Therefore, indeed, at elevated temperatures, the process of plastics decomposition dominates, whereas at lower temperatures the textile and *rest* fractions decomposition is widely observed.

An increase in the CO and CO_2 contents at 400–450 °C can be associated with the decomposition of the wood and paper fractions as well as with lignocellulose-contaminants present in other fractions. Indeed, the lignocellulosic materials decomposition is mainly connected with the CO and CO_2 production (Jagodzińska et al., 2020; Sophonrat et al., 2019). CO and CO_2 production can be also related to the decomposition of polyurethane foam present in the *rest* fraction (Garrido and Font, 2015). Additionally, the high contents of CH_4, H_2 and C_2–C_4 gases at 400–450 °C can be attributed to the decomposition of tires and other rubber-materials (Elbaba et al., 2010) as well as to the textiles and plastics decomposition (Nahil and Williams, 2010; Williams and Williams, 1999a). Therefore, it can be concluded that at lower temperatures, the non-condensables composition can be predominantly attributed to the decomposition of the *rest* and textile fractions, followed by the decomposition of the wood and paper and partial decomposition of plastics.

At higher temperatures (500–600 °C), decomposition of plastic fractions (so-called 2D and 3D plastics) dominates. The PE (dominating in 2D plastics) decomposition is connected to the C_2H_6, C_2H_4, and C_4H_{10} production (Zaini et al., 2019). As a result, an increase in the C_2 gases content can be seen. Furthermore, an increased CH_4 production at 550 °C can be linked to the PS (dominating in 3D plastics) decomposition (Zaini et al., 2019). At the elevated temperature (700 °C), secondary cracking can be observed as indicated by the decrease of the C_4 and C_3 gas yields in favour of the CH_4 and C_2 gas yields, which coincides with the findings of (Buah et al., 2007).

Three primary sources of H_2S in non-condensables can be detected, namely rubber (vulcanised), textiles (sulphur-dying), and sulphur-contaminants in other fractions. However, no overall tendency can be seen with respect to the H_2S content in the non-condensables.

The non-condensables average gross calorific value is 43.12 MJ/m^3_n (excluding C_4 gases from the calculation). This high value is connected with the relatively high content of energy-rich hydrocarbons. The produced non-condensables can be considered as substitutes of natural gas with respect to the thermal input to

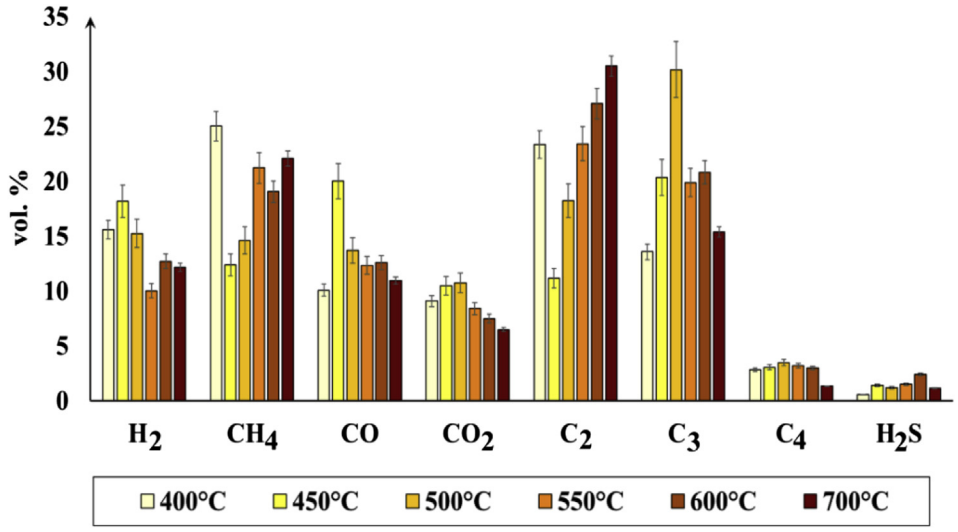

Fig. 4. Non-condensables composition at different pyrolysis temperatures.

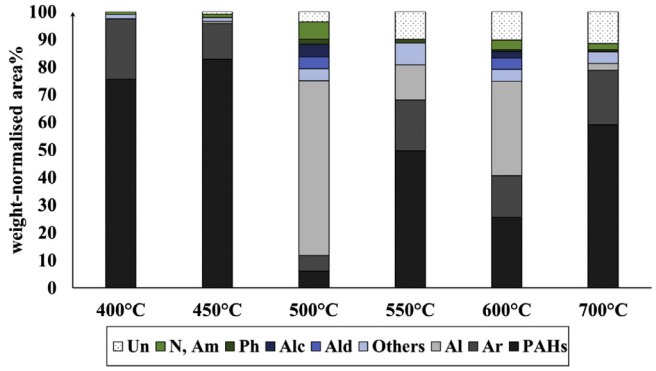

Fig. 5. Condensables compositions at different pyrolysis temperatures (Un – unknown; N, Am – nitrates, amides; Ph – phenols; Alc – alcohols; Ald – aldehydes; Al – aliphatic compounds; Ar – aromatic compounds; PAHs – polycyclic aromatic hydrocarbons).

combustion equipment (Honus et al., 2018). Nevertheless, it has to be noted that the yield (volume and mass) of the produced non-condensables is not high; therefore, the favourable mechanism of the gas utilisation has to be subjected to further economic analyses.

3.3. Condensables composition

Fig. 5 shows the condensables composition at different pyrolysis temperatures. The exact values are shown in Table A3 in the Supplementary material. The detected compounds were divided into nine main groups; the list of the main detected compounds within those groups can be found in Table A4-6 in the Supplementary material. The group named *Others* consist of, among others, thianes, thiopenes, quinolones and esters. The peaks of unidentifiable (due to the missing spectras of chromatographic data) or mixed hydrocarbons are marked as *Unknown* (Un). Their content increases along with the temperature as the complexity of the condensables increases. This tendency is a direct consequence of a greater interaction between the formed compounds at the elevated temperatures.

Table 3 shows five main compounds found in the condensables, along with their content altogether. The results do not show one overall tendency, which is a direct consequence of the feedstock's complex decomposition pattern. Nevertheless, similarly to the results for non-condensables, there is a noticeable change in the decomposition nature at 500 °C.

At lower temperatures (400–450 °C), polycyclic aromatic hydrocarbons (PAHs) dominate in the condensables, representing 75–83% of the total measured weight-normalised area. This tendency coincides with the available data for health-care waste (Mohseni-Bandpei et al., 2019), where PAHs also dominate among the condensables. The common point between those waste and the analysed feedstock is that in both cases the plastic fraction dominates, followed by a relatively high content of textiles; therefore, those two fractions seem to be the primary source of PAHs. Indeed, in our study, the textiles decomposition occurs at 400 °C. It is indicated by nitrates and amides detected in the condensables (Fig. 5), which are considered to be typical products of a synthetic fibre decomposition (Goodman, 1955; Nahil and Williams, 2010). Furthermore, the decomposition of the plastic can be seen at lower temperatures as well.

At 400 °C, anthracene is a predominant compound, representing 21% of the total measured weight-normalised area (Table 3). (Lu and Mulholland, 2004) proposed the mechanism of the formation of anthracene from pyrolysis of a cyclopentadiene, indene, and naphthalene mixture (CPD-I-N). Cyclopentadiene, however, was not detected in the condensables, on the contrary to indene and napthtalene. The presence of indene and napthtalene suggest that the CPD-I-N reaction occurred, which results in that cyclopentadiene was entirely consumed. Indene is a product of the PS and PVC decomposition (Zhou et al., 2015); therefore, its occurrence suggests that the decomposition of those plastics also started at 400 °C.

At 450 °C, phenanthrene and azulene dominate in the condensables (each of 13–14% of the total measured weight-normalised area). Both of those compounds are considered to be mainly derived from a PVC pyrolysis (Anuar Sharuddin et al., 2016; Zhou et al., 2015); thus, 450 °C can be marked as the temperature of an extensive PVC decomposition. This is also confirmed by the study of (Sørum et al., 2001) showing the two-stage PVC decomposition, where the second stage is associated with the remaining hydrocarbons degradation, and the maximum mass loss during this stage occurs at 450 °C. On the other hand, the first stage is associated with the chlorine release.

The high content of phenanthrene at 450 °C can also be

Table 3
The main components detected in the condensables.

Temperature	400 °C	450 °C	500 °C
	Anthracene	Phenanthrene	Nonadec-1-ene
	Pyrene	Azulene	Heptadec-15-enal
	Naphthalene	Pyrene	Heptadec-3-ene
	Fluoranthene	Fluoranthene	Pentadec-1-ene
	Biphenylene	Triphenylene	Hexadec-7-ene
Content altogether, weight-normalised area%	53.6	54.4	16.6
Temperature	**550°C**	**600°C**	**700°C**
	Toluene	Tetradec-1-ene	Anthracene
	Anthracene	Hexadec-1-ene	Biphenylene
	Styrene	Octadec-1-ene	Pyrene
	Methyl 2,5-dichlorobenzoate	Hexadec-14-enal	1,1′-Biphenyl
	Ethylbenzene	Tridec-1-ene	Naphthalene
Content altogether, weight-normalised area%	18	11.5	28.9

associated with the decrease of the C_2 gas concentrations (more precisely – ethene) in the non-condensables at the same temperature (Fig. 4 and Table A2 in the Supplementary material). Ethene (C_2H_4) decomposes to vinyl radicals (C_2H_3) at higher temperatures (Shukla and Koshi, 2012). (Kislov et al., 2013) proposed the mechanism, utilising these vinyl radicals, which leads to a formation of phenanthrene from acenaphthalene by attaching a vinyl group to it. Therefore, the phenanthrene formation combined additionally with the enhanced fluoroanthene formation by the HAVA (hydrogen-abstraction/vinyl-addition) mechanism (Shukla and Koshi, 2012), significantly increased the demand for vinyl radicals, and, consequently, caused the decrease of the C_2H_4 concentration in the non-condensables.

Moreover, the start of the formation of thiopenes and quinolines was observed at 450 °C. Thiopenes are considered to be classic products of sulphur cross-linked rubber pyrolysis (Kaminsky and Mennerich, 2001; Wang et al., 2014), whereas an abundance of quinolones can be found among natural rubber tyre pyrolysis products (Kan et al., 2017); therefore, their formation suggests a start of the decomposition of the *rest* fraction, which contains rubber.

Given the above, it can be concluded that the temperature range of 400–450 °C corresponds mainly to the decomposition of textiles, rubber (the *rest* fraction), PVC as well as, partially, the decomposition of PS.

At 500 °C, the decomposition nature changes. The composition of condensables becomes more complex, as evidenced by the total content of five main components shown in Table 3 – this content noticeably decreases at 500 °C, and this tendency remains until a temperature of 700 °C is reached. The high content of aliphatic compounds (Fig. 5), among which long-chain alkenes (C_{10}–C_{23}) dominate, followed by alkanes, indicates intensive PE decomposition, as those compounds are typical products of its pyrolysis (Sophonrat et al., 2017).

A distinct content of nitriles, amides, alcohols, and aldehydes can be observed at 500 °C as well. As mentioned before, the nitriles and amides formation is connected mostly with textiles decomposition. On the other hand, higher contents of alcohols and aldehydes accompanied by the presence of phenols may seemingly indicate decomposition of lignocellulosic material as those are typical products of this process (Jagodzińska et al., 2019a). These compounds, however, were not observed at lower temperatures. This excludes biomass or any other organic material as the source of oxygenated compounds as their decomposition starts at lower temperatures than 400 °C (Ratnasari et al., 2019). This points at possible PET presence in the sample as its decomposition results in the formation of ketones and aldehydes (Diaz Silvarrey and Phan, 2016; Williams and Williams, 1999a).

A further decomposition of PE can be observed ending at 600 °C. At 550 °C, however, extensive decomposition of PS can also be observed as indicated by the high content of styrene (Table 3) - the main product of the process (Anuar Sharuddin et al., 2016; Sophonrat et al., 2017). Consequently, the parallel decomposition of PE and PS results in the intensification of aromatic compounds (mainly benzene derivatives) and PAHs formation at 550 °C. This tendency coincides with the study of (Williams and Williams, 1999a), which showed that mixing of those two types of plastics triggered the formation of aromatics and PAHs. The aromatisation of lighter hydrocarbons (Diels–Alder reactions) leads to the formation of alkyloaromatics (Blanco et al., 2012), such as toluene which dominated in the analysed condensables (Table 3). The enhanced production of toluene is in line with the study of (Williams and Williams, 1999a) as well.

At 700 °C, two benzene derivatives dominate along with three PAHs (Table 3) and almost no aliphatics can be seen (Fig. 5). This tendency is a result of the secondary reactions of primary pyrolysis products (Constantinidis et al., 2015; Guan et al., 2008; Jacobelli et al., 1983), the aforementioned secondary Diels–Alder reactions (Zhou et al., 2015) and the secondary thermal cracking (Williams and Williams, 1999b) intensified at elevated temperatures. A similar trend can be observed in the study of (Zaini et al., 2019), who subjected RDF from excavated materials to pyrolysis at 900 °C and obtained condensables with a very high content of aromatic compounds.

Given the above, it can be concluded that the temperature range of 500–600 °C corresponds primarily to the PE and PS decomposition. At 700 °C, however, the condensables are subjected to the secondary reactions and cracking, which are triggered by the high temperature.

The characteristic of condensables varies with temperature change. Therefore, the further assessment of their possible application shall be done separately for each temperature range. For instance, the obtained waxes at 500 and 600 °C are not of commercial interest in a raw state; however, they are characterised by a relatively high potential of catalytic upgrading to fuels or high-quality syngas (Erkiaga et al., 2015), as olefins show the moderate effect on catalyst deactivation (Barbarias et al., 2016).

3.4. C, H, S, Cl balance

Fig. 6 shows C, H, N, O, Cl and S distribution among the pyrolysis products at different temperatures in relation to their initial contents in the feedstock. The measured elemental composition and ash content in the char are shown in Table A7 in the Supplementary

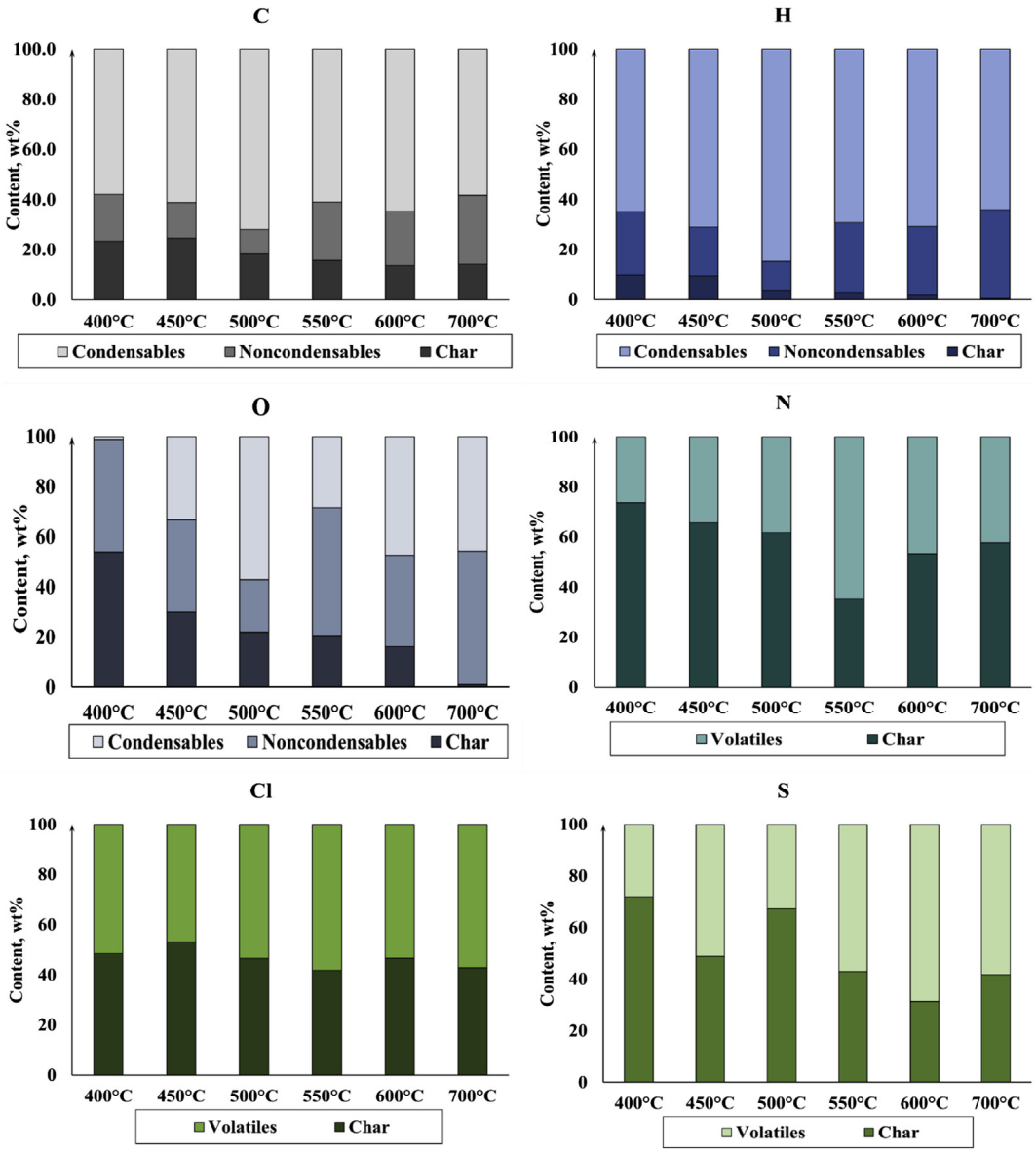

Fig. 6. C, H, O, N, Cl, S distributions for the pyrolysis products at different temperatures (normalised to the initial content in the feedstock); for N, Cl and S condensables and non-condensables are referred to collectively as volatiles.

material. The element contents in condensables were calculated as the difference between the initial element mass in the feedstock and the sum of contents in the other pyrolysis products. Moreover, the nitrogen content could not be measured in non-condensables (due to that nitrogen was used as a carrier gas); therefore, the results for N in the condensables and non-condensables are shown collectively as volatiles. The measured content of chlorine in non-condensables was very low (in the range of 1–2 wt%) as well as the calculated content of sulphur in condensables. Therefore, similarly to for N, the results for S and Cl in the non-condensables and condensables were shown collectively as volatiles.

The progressive increase of the temperature results in a decrease of the C and H contents in the char in favour of, mostly, condensables. On the other hand, the nitrogen content in the char is relatively stable and does not show any overall tendency with one exception of the decrease at 550 °C. This decrease is not reflected in the condensables composition (no increase in nitriles and amides content); therefore, it can be attributed to the growth of the nitrogen content in the non-condensables. The decrease in the C and H contents and the relative stable N content agree with the results of (Buah et al., 2007; Yang et al., 2018). Similarly to the nitrogen content, the oxygen content does not show any overall tendency as the temperature is changed. The increase of the O content in the condensables at 500 °C can be linked to the rise of the oxygenated compounds content, as discussed previously in paragraph *3.3. Condensables composition* (Fig. 5).

The content of Cl in the char is relatively stable along as the temperature changes. Since the chlorine content in the non-condensables is low, it can be concluded that Cl tends to form organic chlorine compounds rather than gaseous HCl. On the contrary (Fekhar et al., 2019), reported an extensive formation of gaseous chlorine compounds and the small content of chlorine in solid and condensable products of pyrolysis. That difference can be attributed to the compositional and structural difference between excavated and fresh waste, reflected by higher chlorine content in the excavated waste due to its preconcentration (Rotheut and

Quicker, 2017).

The fluctuations of the sulphur contents are noticeable. However, they follow the tendency of the H_2S content in the non-condensables (Fig. 4). Therefore, since the sulphur content in the condensables is small, and the changes of the S content in the char follows the tendency of forming H_2S, it can be concluded that sulphur tends to form gaseous compounds rather than organic sulphur compounds.

4. Conclusions

The knowledge gap on excavated waste pyrolysis motivated the study. The refuse-derived fuel (RDF) formed from excavated waste was subjected to pyrolysis at six temperatures in the range of 400–700 °C. The temperature impact on the quality of the process products was determined. Overall, the main findings of the study can be summarised as follows:

1. The thermogravimetric (TG) and derivative thermogravimetric (DTG) degradation profiles do not coincide with the degradation profile in the lab-scale pyrolysis reactor, due to a thermal lag caused by a high soil-like fraction content.
2. The feedstock complex composition results in a complex thermal decomposition pattern. Consequently, no overall tendency with respect to the non-condensables and the condensables composition can be determined within a temperature change. However, lower temperatures (400–450 °C) can be associated with the decomposition of textiles and the so-called *rest* fraction, whereas the PE and PS decomposition dominates at 500–600 °C. At 700 °C, thermal cracking can be observed coupled with secondary reactions, inter alia Diels–Alder reactions.
3. The non-condensables are characterised by relatively high gross calorific values (average of 43.12 MJ/m^3_n) due to the relatively high content of C_2–C_3 hydrocarbons. However, the relatively high content of H_2S in the non-condensables may pose a risk of corrosion during transportation and combustion.
4. The condensables contain mostly polycyclic aromatic hydrocarbons (PAHs) at 400–450 °C (on average, 79% of the total weight-normalised area) and at higher temperatures, the content of aliphatic (mostly olefins) increases with the temperature and reaches maximum value at 500 °C (63% of the total weight-normalised area) due to an extensive PE decomposition.
5. Chlorine tends to form organic compounds rather than gaseous HCl, whereas sulphur tends to form gaseous compounds (like H_2S) rather than organic sulphur compounds. These tendencies are crucial to consider for a further assessment of the process products utilisation.

Given the above, further studies following two paths shall be considered: I – the feasibility evaluation of the catalytic upgrading of pyrovapours from excavated waste pyrolysis and II – the further research on the char characterisation to determine its possible applications.

CRediT authorship contribution statement

Katarzyna Jagodzińska: Conceptualization, Methodology, Investigation, Resources, Writing - original draft, Writing - review & editing. **Ilman Nuran Zaini:** Resources, Writing - review & editing. **Rikard Svanberg:** Resources, Writing - review & editing. **Weihong Yang:** Supervision, Writing - review & editing. **Pär Göran Jönsson:** Supervision, Writing - review & editing.

Declaration of competing interest

The authors declare that they have no known competing financial interests or personal relationships that could have appeared to influence the work reported in this paper.

Acknowledgement

The NEW-MINE project has received funding from the European Union's Horizon 2020 research and innovation programme under the Marie Skłodowska-Curie grant agreement No 721185. The project website is http://new-mine.eu/.

Appendix A. Supplementary data

Supplementary data to this article can be found online at https://doi.org/10.1016/j.jclepro.2020.123541.

References

Agon, N., Hrabovský, M., Chumak, O., Hlína, M., Kopecký, V., Mašláni, A., Bosmans, A., Helsen, L., Skoblja, S., Van Oost, G., Vierendeels, J., 2016. Plasma gasification of refuse derived fuel in a single-stage system using different gasifying agents. Waste Manag. 47, 246–255. https://doi.org/10.1016/j.wasman.2015.07.014.

Anuar Sharuddin, S.D., Abnisa, F., Wan Daud, W.M.A., Aroua, M.K., 2016. A review on pyrolysis of plastic wastes. Energy Convers. Manag. 115, 308–326. https://doi.org/10.1016/j.enconman.2016.02.037.

Barbarias, I., Lopez, G., Artetxe, M., Arregi, A., Santamaria, L., Bilbao, J., Olazar, M., 2016. Pyrolysis and in-line catalytic steam reforming of polystyrene through a two-step reaction system. J. Anal. Appl. Pyrolysis 122, 502–510. https://doi.org/10.1016/j.jaap.2016.10.006.

Blanco, P.H., Wu, C., Onwudili, J.A., Williams, P.T., 2012. Characterization of tar from the pyrolysis/gasification of refuse derived Fuel : influence of process parameters and catalysis. Energy Fuels 26, 2107–2115. https://doi.org/10.1021/ef300031j.

Bosmans, A., De Dobbelaere, C., Helsen, L., 2014. Pyrolysis characteristics of excavated waste material processed into refuse derived fuel. Fuel 122, 198–205. https://doi.org/10.1016/j.fuel.2014.01.019.

Bosmans, A., Vanderreydt, I., Geysen, D., Helsen, L., 2013. The crucial role of Waste-to-Energy technologies in enhanced landfill mining: a technology review. J. Clean. Prod. 55, 10–23. https://doi.org/10.1016/j.jclepro.2012.05.032.

Breyer, S., Mekhitarian, L., Rimez, B., Haut, B., 2017. Production of an alternative fuel by the co-pyrolysis of landfill recovered plastic wastes and used lubrication oils. Waste Manag. 60, 363–374. https://doi.org/10.1016/j.wasman.2016.12.011.

Buah, W.K., Cunliffe, A.M., Williams, P.T., 2007. Characterization of products from the pyrolysis of municipal solid waste. Process Saf. Environ. Protect. 85, 450–457. https://doi.org/10.1205/psep07024.

Canopoli, L., Coulon, F., Wagland, S.T., 2020. Degradation of excavated polyethylene and polypropylene waste from landfill. Sci. Total Environ. 698, 134125. https://doi.org/10.1016/j.scitotenv.2019.134125.

Canopoli, L., Fidalgo, B., Coulon, F., Wagland, S.T., 2018. Physico-chemical properties of excavated plastic from landfill mining and current recycling routes. Waste Manag. 76, 55–67. https://doi.org/10.1016/j.wasman.2018.03.043.

Chen, D., Yin, L., Wang, H., He, P., 2015. Reprint of: pyrolysis technologies for municipal solid waste: a review. Waste Manag. 37, 116–136. https://doi.org/10.1016/j.wasman.2015.01.022.

Constantinidis, P., Schmitt, H.C., Fischer, I., Yan, B., Rijs, A.M., 2015. Formation of polycyclic aromatic hydrocarbons from bimolecular reactions of phenyl radicals at high temperatures. Phys. Chem. Chem. Phys. 17, 29064–29071. https://doi.org/10.1039/c5cp05354d.

Danthurebandara, M., Van Passel, S., Vanderreydt, I., Van Acker, K., 2015. Environmental and economic performance of plasma gasification in Enhanced Landfill Mining. Waste Manag. 45, 458–467. https://doi.org/10.1016/j.wasman.2015.06.022.

Diaz Silvarrey, L.S., Phan, A.N., 2016. Kinetic study of municipal plastic waste. Int. J. Hydrogen Energy 41, 16352–16364. https://doi.org/10.1016/j.ijhydene.2016.05.202.

Elbaba, I.F., Wu, C., Williams, P.T., 2010. Catalytic pyrolysis-gasification of waste tire and tire elastomers for hydrogen production. Energy Fuels 24, 3928–3935. https://doi.org/10.1021/ef100317b.

Erkiaga, A., Lopez, G., Barbarias, I., Artetxe, M., Amutio, M., Bilbao, J., Olazar, M., 2015. HDPE pyrolysis-steam reforming in a tandem spouted bed-fixed bed reactor for H2 production. J. Anal. Appl. Pyrolysis 116, 34–41. https://doi.org/10.1016/j.jaap.2015.10.010.

European Commission, 2011. Roadmap to a Resource Efficient Europe - COM(2011)

571 Final.
Fekhar, B., Gombor, L., Miskolczi, N., 2019. Pyrolysis of chlorine contaminated municipal plastic waste: in-situ upgrading of pyrolysis oils by Ni/ZSM-5, Ni/SAPO-11, red mud and Ca(OH)2 containing catalysts. J. Energy Inst. 92, 1270–1283. https://doi.org/10.1016/j.joei.2018.10.007.
Forster, G.A., 1995. Assessment of Landfill Reclamation and the Effects of Age on the Combustion of Recovered Municipal Solid Waste (NRELfTP-430-7449). Colorado, U.S.A.
Garcia Lopez, C., Ni, A., Parrodi, J.C.H., Küppers, B., Raulf, K., Pretz, T., 2019. Characterization of landfil mining material after ballistic separation to evaluate material and energy recovery potential. Detritus 8, 5–23. https://doi.org/10.31025/2611-4135/2019.13780.
Garrido, M.A., Font, R., 2015. Pyrolysis and combustion study of flexible polyurethane foam. J. Anal. Appl. Pyrolysis 113, 202–215. https://doi.org/10.1016/j.jaap.2014.12.017.
Goodman, I., 1955. The thermal degradation of 66 nylon: further studies on the pyrolysis of di-n- butyl adipamide. J. Polym. Sci. 17, 4–7. https://doi.org/10.1002/pol.1955.120178610.
Guan, G., Metzke, D., Jiang, M., Löwe, H., 2008. High temperature reactions in microstructured reactors - synthesis of biphenyl by pyrolysis of benzene. In: 2008 AIChE Spring National Meeting, Conference Proceedings.
He, P., Chen, L., Shao, L., Zhang, H., Lü, F., 2019. Municipal solid waste (MSW) landfill: a source of microplastics? -Evidence of microplastics in landfill leachate. Water Res. 159, 38–45. https://doi.org/10.1016/j.watres.2019.04.060.
Hogland, W., Marques, M., Nimmermark, S., 2004. Landfill mining and waste characterization: a strategy for remediation of contaminated areas. J. Mater. Cycles Waste Manag. 6, 119–124. https://doi.org/10.1007/s10163-003-0110-x.
Honus, S., Kumagai, S., Fedorko, G., Molnár, V., Yoshioka, T., 2018. Pyrolysis gases produced from individual and mixed PE, PP, PS, PVC, and PET—Part I: production and physical properties. Fuel 221, 346–360. https://doi.org/10.1016/j.fuel.2018.02.074.
Hwang, I.H., Kobayashi, J., Kawamoto, K., 2014. Characterization of products obtained from pyrolysis and steam gasification of wood waste, RDF, and RPF. Waste Manag. 34, 402–410. https://doi.org/10.1016/j.wasman.2013.10.009.
Jacobelli, C., Perez, G., Polcaro, C., Possagno, E., Bassanelli, R., Lilla, E., 1983. Formation of isomeric terphenyls and triphenylene by pyrolysis of benzene. J. Anal. Appl. Pyrolysis 5, 237–243. https://doi.org/10.1016/0165-2370(83)80030-8.
Jagodzińska, K., Czerep, M., Kudlek, E., Wnukowski, M., Pronobis, M., Yang, W., 2020. Torrefaction of agricultural residues: effect of temperature and residence time on the process products properties. J. Energy Resour. Technol. 142 (7) https://doi.org/10.1115/1.4046275.
Jagodzińska, K., Czerep, M., Kudlek, E., Wnukowski, M., Yang, W., 2019a. Torrefaction of wheat-barley straw: composition and toxicity of torrefaction condensates. Biomass Bioenergy 129, 105335. https://doi.org/10.1016/j.biombioe.2019.105335.
Jagodzińska, K., Mroczek, K., Nowińska, K., Gołombek, K., Kalisz, S., 2019b. The impact of additives on the retention of heavy metals in the bottom ash during RDF incineration. Energy 183, 854–868. https://doi.org/10.1016/j.energy.2019.06.162.
Johansson, N., Krook, J., Eklund, M., 2012. Transforming dumps into gold mines. Experiences from Swedish case studies. Environ. Innov. Soc. Transitions 5, 33–48. https://doi.org/10.1016/j.eist.2012.10.004.
Jones, P.T., Geysen, D., Tielemans, Y., Van Passel, S., Pontikes, Y., Blanpain, B., Quaghebeur, M., Hoekstra, N., 2013. Enhanced Landfill Mining in view of multiple resource recovery: a critical review. J. Clean. Prod. 55, 45–55. https://doi.org/10.1016/j.jclepro.2012.05.021.
Kaartinen, T., Sormunen, K., Rintala, J., 2013. Case study on sampling, processing and characterization of landfilled municipal solid waste in the view of landfill mining. J. Clean. Prod. 55, 56–66. https://doi.org/10.1016/j.jclepro.2013.02.036.
Kaminsky, W., Mennerich, C., 2001. Pyrolysis of synthetic tire rubber in a fluidised-bed reactor to yield 1,3-butadiene, styrene and carbon black. J. Anal. Appl. Pyrolysis 58 (59), 803–811. https://doi.org/10.1016/S0165-2370(00)00129-7.
Kamura, K., Omori, M., Kurokawa, M., Tanaka, H., 2019. Estimation of the potential of landfill mining and exploration of metal-enriched zones. Waste Manag. 93, 122–129. https://doi.org/10.1016/j.wasman.2019.04.050.
Kan, T., Strezov, V., Evans, T., 2017. Fuel production from pyrolysis of natural and synthetic rubbers. Fuel 191, 403–410. https://doi.org/10.1016/j.fuel.2016.11.100.
Kislov, V.V., Sadovnikov, A.I., Mebel, A.M., 2013. Formation mechanism of polycyclic aromatic hydrocarbons beyond the second aromatic ring. J. Phys. Chem. 117, 4794–4816. https://doi.org/10.1021/jp402481y.
Krook, J., Svensson, N., Eklund, M., 2012. Landfill mining: a critical review of two decades of research. Waste Manag. 32, 513–520. https://doi.org/10.1016/j.wasman.2011.10.015.
Lokahita, B., Samudro, G., Huboyo, H.S., Aziz, M., Takahashi, F., 2019. Energy recovery potential from excavating municipal solid waste dumpsite in Indonesia. Energy Procedia 158, 243–248. https://doi.org/10.1016/j.egypro.2019.01.083.
Lu, M., Mulholland, J.A., 2004. PAH Growth from the pyrolysis of CPD, indene and naphthalene mixture. Chemosphere 55, 605–610. https://doi.org/10.1016/j.chemosphere.2003.12.002.
Manyà, J.J., García-Ceballos, F., Azuara, M., Latorre, N., Royo, C., 2015. Pyrolysis and char reactivity of a poor-quality refuse-derived fuel (RDF) from municipal solid waste. Fuel Process. Technol. 140, 276–284. https://doi.org/10.1016/j.fuproc.2015.09.014.
Mohseni-Bandpei, A., Majlesi, M., Rafiee, M., Nojavan, S., Nowrouz, P., Zolfagharpour, H., 2019. Polycyclic aromatic hydrocarbons (PAHs) formation during the fast pyrolysis of hazardous health-care waste. Chemosphere 227, 277–288. https://doi.org/10.1016/j.chemosphere.2019.04.028.
Montané, D., Abelló, S., Farriol, X., Berrueco, C., 2013. Volatilization characteristics of solid recovered fuels (SRFs). Fuel Process. Technol. 113, 90–96. https://doi.org/10.1016/j.fuproc.2013.03.026.
Nahil, M.A., Williams, P.T., 2010. Activated carbons from acrylic textile waste. J. Anal. Appl. Pyrolysis 89, 51–59. https://doi.org/10.1016/j.jaap.2010.05.005.
Nobre, C., Vilarinho, C., Alves, O., Mendes, B., Gonçalves, M., 2019. Upgrading of refuse derived fuel through torrefaction and carbonization: evaluation of RDF char fuel properties. Energy 181, 66–76. https://doi.org/10.1016/j.energy.2019.05.105.
Quaghebeur, M., Laenen, B., Geysen, D., Nielsen, P., Pontikes, Y., Van Gerven, T., Spooren, J., 2013. Characterization of landfilled materials: screening of the enhanced landfill mining potential. J. Clean. Prod. 55, 72–83. https://doi.org/10.1016/j.jclepro.2012.06.012.
Ratnasari, D.K., Horn, A., Brunner, T., Yang, W., Jönsson, P.G., 2019. The thermal degradation of lignocellulose biomass with an acid leaching pre-treatment using a H-ZSM-5/Al-MCM-41 catalyst mixture. Fuel 257, 116086. https://doi.org/10.1016/j.fuel.2019.116086.
Rotheut, M., Quicker, P., 2017. Energetic utilisation of refuse derived fuels from landfill mining. Waste Manag. 62, 101–117. https://doi.org/10.1016/j.wasman.2017.02.002.
Shukla, B., Koshi, M., 2012. A novel route for PAH growth in HACA based mechanisms. Combust. Flame 159, 3589–3596. https://doi.org/10.1016/j.combustflame.2012.08.007.
Sieradzka, M., Rajca, P., Zajemska, M., Mlonka-Mędrala, A., Magdziarz, A., 2020. Prediction of gaseous products from refuse derived fuel pyrolysis using chemical modelling software - ansys Chemkin-Pro. J. Clean. Prod. 248 https://doi.org/10.1016/J.JCLEPRO.2019.119277.
Singh, A., Chandel, M.K., 2019. Effect of aging on waste characteristics excavated from an Indian dumpsite and its potential valorisation. Process Saf. Environ. Protect. https://doi.org/10.1016/j.psep.2019.11.025.
Sophonrat, N., Sandström, L., Johansson, A.C., Yang, W., 2017. Co-pyrolysis of mixed plastics and cellulose: an interaction study by Py-GC×GC/MS. Energy Fuels 31, 11078–11090. https://doi.org/10.1021/acs.energyfuels.7b01887.
Sophonrat, N., Sandström, L., Svanberg, R., Han, T., Dvinskikh, S., Lousada, C.M., Yang, W., 2019. Ex situ catalytic pyrolysis of a mixture of Polyvinyl chloride and cellulose using calcium oxide for HCl adsorption and catalytic reforming of the pyrolysis products. Ind. Eng. Chem. Res. 58, 13960–13970. https://doi.org/10.1021/acs.iecr.9b02299.
Sørum, L., Grønli, M.G., Hustad, J.E., 2001. Pyrolysis characteristics and kinetics of municipal solid waste. Fuel 80, 1217–1227.
Wang, W.L., Chang, J.M., Cai, L.P., Shi, S.Q., 2014. Quality improvement of pyrolysis oil from waste rubber by adding sawdust. Waste Manag. 34, 2603–2610. https://doi.org/10.1016/j.wasman.2014.08.016.
Williams, P.T., Williams, E.A., 1999a. Interaction of plastics in mixed-plastics pyrolysis. Energy Fuels 13, 188–196. https://doi.org/10.1021/ef980163x.
Williams, P.T., Williams, E.A., 1999b. Fluidised bed pyrolysis of low density polyethylene to produce petrochemical feedstock. J. Anal. Appl. Pyrolysis 51, 107–126. https://doi.org/10.1016/S0165-2370(99)00011-X.
Ximenes, F.A., Cowie, A.L., Barlaz, M.A., 2018. The decay of engineered wood products and paper excavated from landfills in Australia. Waste Manag. 74, 312–322. https://doi.org/10.1016/j.wasman.2017.11.035.
Yang, Y., Heaven, S., Venetsaneas, N., Banks, C.J., Bridgwater, A.V., 2018. Slow pyrolysis of organic fraction of municipal solid waste (OFMSW): characterisation of products and screening of the aqueous liquid product for anaerobic digestion. Appl. Energy 213, 158–168. https://doi.org/10.1016/j.apenergy.2018.01.018.
Yi, S., 2019. Resource recovery potentials by landfill mining and reclamation in South Korea. J. Environ. Manag. 242, 178–185. https://doi.org/10.1016/j.jenvman.2019.01.101.
Zaini, I.N., García López, C., Pretz, T., Yang, W., Jönsson, P.G., 2019. Characterization of pyrolysis products of high-ash excavated-waste and its char gasification reactivity and kinetics under a steam atmosphere. Waste Manag. 97, 149–163. https://doi.org/10.1016/j.wasman.2019.08.001.
Zhou, C., Fang, W., Xu, W., Cao, A., Wang, R., 2014. Characteristics and the recovery potential of plastic wastes obtained from landfill mining. J. Clean. Prod. 80, 80–86. https://doi.org/10.1016/j.jclepro.2014.05.083.
Zhou, H., Wu, C., Onwudili, J.A., Meng, A., Zhang, Y., Williams, P.T., 2015. Polycyclic aromatic hydrocarbons (PAH) formation from the pyrolysis of different municipal solid waste fractions. Waste Manag. 36, 136–146. https://doi.org/10.1016/j.wasman.2014.09.014.